INTERFACE

royalsocietypublishing.org/journal/rsif

Research

Cite this article: Bobadilla AVP, Arévalo J, Sarró E, Byrne HM, Maini PK, Carraro T, Balocco S, Meseguer A, Alarcón T. 2019 *In vitro* cell migration quantification method for scratch assays. *J. R. Soc. Interface* **16**: 20180709. http://dx.doi.org/10.1098/rsif.2018.0709

Received: 21 September 2018
Accepted: 21 January 2019

Subject Category:
Life Sciences–Mathematics interface

Subject Areas:
biomathematics, bioinformatics, computational biology

Keywords:
scratch assays, migration quantification methods, migration rates

Author for correspondence:
Ana Victoria Ponce Bobadilla
e-mail: anavictoria.ponce@iwr.uni-heidelberg.de

Electronic supplementary material is available online at https://dx.doi.org/10.6084/m9.figshare.c.4381946.

THE ROYAL SOCIETY PUBLISHING

In vitro cell migration quantification method for scratch assays

Ana Victoria Ponce Bobadilla[1,2], Jazmine Arévalo[3], Eduard Sarró[3], Helen M. Byrne[4], Philip K. Maini[4], Thomas Carraro[1,2], Simone Balocco[5,6], Anna Meseguer[3,7,8] and Tomás Alarcón[9,10,11,12]

[1]Institute for Applied Mathematics, Heidelberg University, 69120 Heidelberg, Germany
[2]Interdisciplinary Center for Scientific Computing (IWR), Heidelberg University, 69120 Heidelberg, Germany
[3]Renal Physiopathology Group, CIBBIM-Nanomedicine, Vall d'Hebron Research Institute, Barcelona, Spain
[4]Wolfson Centre for Mathematical Biology, Mathematical Institute, University of Oxford, Oxford OX2 6GG, UK
[5]Department of Mathematics and Informatics, University of Barcelona, Gran Via 585, 08007 Barcelona, Spain
[6]Computer Vision Center, 08193 Bellaterra, Spain
[7]Departament de Bioquímica i Biologia Molecular, Unitat de Bioquímica de Medicina, Universitat Autònoma de Barcelona, Bellaterra, Spain
[8]Red de Investigación Renal (REDINREN), Instituto Carlos III-FEDER, Madrid, Spain
[9]ICREA, Pg. Lluís Companys 23, 08010 Barcelona, Spain
[10]Centre de Recerca Matemàtica, Edifici C, Campus de Bellaterra, 08193 Bellaterra (Barcelona), Spain
[11]Departament de Matemàtiques, Universitat Autònoma de Barcelona, 08193 Bellaterra (Barcelona), Spain
[12]Barcelona Graduate School of Mathematics (BGSMath), Barcelona, Spain

AVPB, 0000-0002-0959-4058; JA, 0000-0002-8824-424X; ES, 0000-0001-7723-2916; HMB, 0000-0003-1771-5910; PKM, 0000-0002-0146-9164; TC, 0000-0002-0503-4555; SB, 0000-0002-7149-7806; TA, 0000-0002-8566-3676

The scratch assay is an *in vitro* technique used to assess the contribution of molecular and cellular mechanisms to cell migration. The assay can also be used to evaluate therapeutic compounds before clinical use. Current quantification methods of scratch assays deal poorly with irregular cell-free areas and crooked leading edges which are features typically present in the experimental data. We introduce a new migration quantification method, called 'monolayer edge velocimetry', that permits analysis of low-quality experimental data and better statistical classification of migration rates than standard quantification methods. The new method relies on quantifying the horizontal component of the cell monolayer velocity across the leading edge. By performing a classification test on *in silico* data, we show that the method exhibits significantly lower statistical errors than standard methods. When applied to *in vitro* data, our method outperforms standard methods by detecting differences in the migration rates between different cell groups that the other methods could not detect. Application of this new method will enable quantification of migration rates from *in vitro* scratch assay data that cannot be analysed using existing methods.

1. Background

Cell migration plays a fundamental role in developing and maintaining the organization of multicellular organisms, while aberrant cell migration is found in many pathological disorders like cancer and atherosclerosis [1,2]. Cell migration involves the movement of individual cells, cell sheets or cell clusters from one location to another [3]. Two main types of migration can be distinguished: single cell migration and collective cell migration. During collective cell migration multiple cells perform a coordinated movement regulated by cell–cell adhesion, collective cell polarization, coordination of cytoskeletal activity and chemical and mechanical cues [1]. *In vitro* assays are central to the study of cell migration since they allow us to quantify cell migratory capacity under controlled experimental conditions [3,4]. The scratch or wound healing assay is the method of choice for studying cell migration due to the low cost

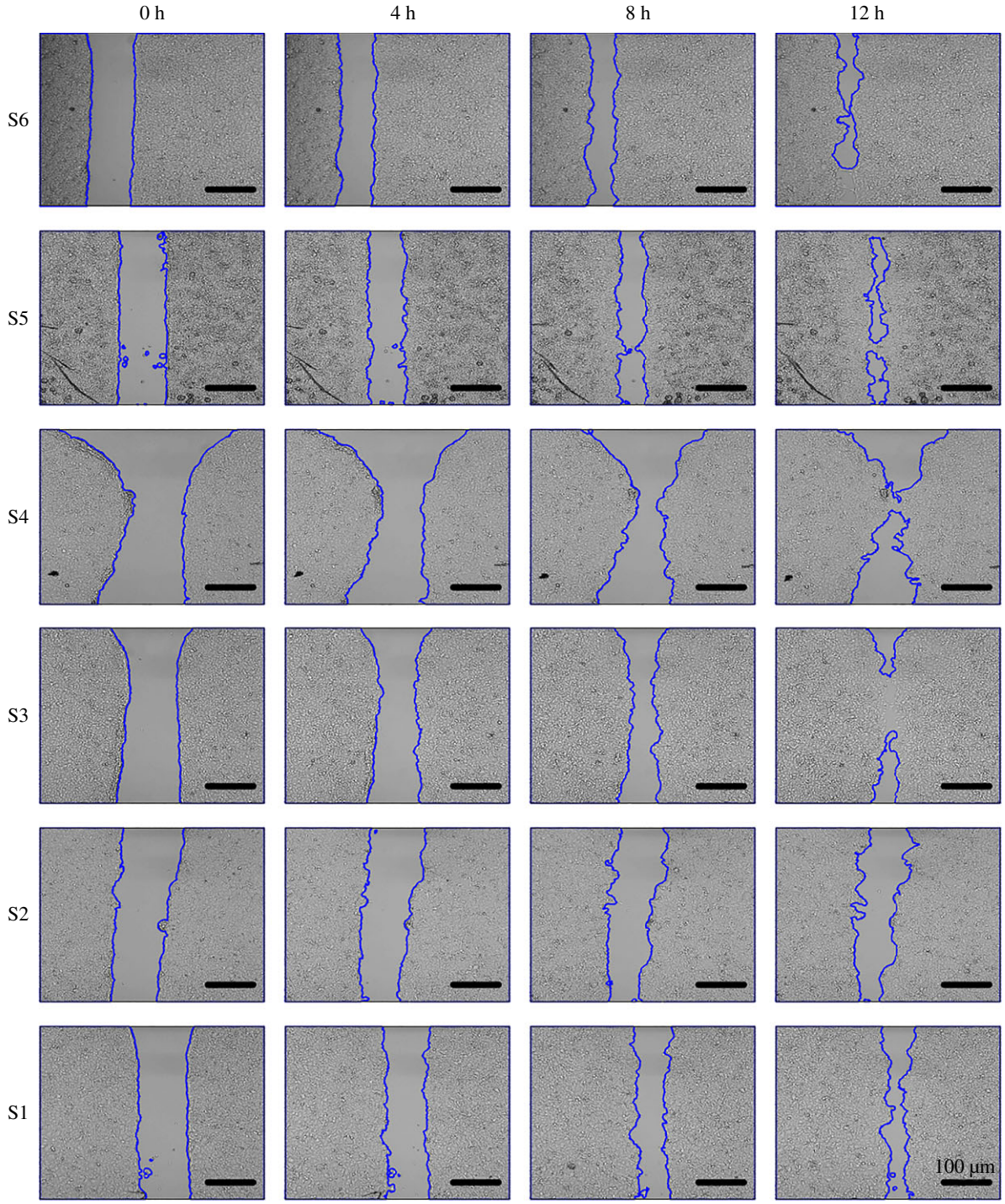

Figure 1. Time-lapse images of a representative scratch assay from each of the six experimental cell groups (S1–S6) are plotted at time 0, 4, 8 and 12 h. In each image, the leading edges were detected by applying the segmentation algorithm. The resulting interfaces/cell fronts are plotted in blue. (Online version in colour.)

and simplicity of its experimental design [4,5]. A scratch assay involves growing a cell monolayer to confluence in a multiwell assay plate; creating a 'wound'—a cell-free zone in the monolayer—into which cells can migrate; and monitoring the recolonization of the scratched region to quantify cell migration [5] (see figure 1). This experimental technique is commonly used to understand the molecular mechanisms that affect cell migration [6,7] and to identify pharmaceutical compounds that can modulate cell migration and consequently drive treatment therapies [8]. Given the key role of scratch assays in biomedical research, it is important to develop robust quantification methods that accurately measure and compare migration rates of different scratch assays.

Multiple quantification methods are used to assess collective cell migration in scratch assays [9]. The most common ones focus on wound width or area change [3,10]. Such methods use a number of metrics to quantify migration, including the percentage difference in the wound width at different time points [7,11], wound width at specific time points [12] and the slope of a linear approximation to the change in wound area [13], among others. Other more computationally intensive methods exist that rely on cell tracking or on determining a velocity field across the full monolayer [14,15]. In this work, we focus on less computationally intensive methods that permit a quick assessment of collective cell migration. A weakness of the aforementioned methods is that they do not perform well when the two borders of the

scratch are not perfectly straight, a feature that is common in experimental data [13,16]. The lack of a reproducible wounding procedure results in non-uniform cell-free areas with irregular leading edges, as can be seen in figure 1. Furthermore, migration rate measurements have been shown to be sensitive to the initial degree of confluence [17] and the initial geometry of the wound [18]. Current quantification methods require high-quality experimental data which are difficult to obtain; therefore, frequently the experimental data are discarded or need to be produced again.

Another issue with existing quantification methods is that many of them use time-specific measurements to determine differences in migration rates of cell samples. Typically, a time point in the course of the experiment is considered at which the wound area or width of each sample is measured. Then, statistical tests are performed on these measurements with the purpose of detecting significant differences [3]. The time points of comparison are not standardized and vary across studies [7,19,20]. Differences in the time points used for comparison may be due to differences in the proliferation rates of the cell types under consideration. The choices are made to minimize the impact of cell proliferation on migration quantification. However, there is no standard procedure for choosing the comparison time even though the choice can affect the comparison and may render the results from the analysis unreliable.

In this work, we introduce a new quantification method that tackles these issues and can be used to analyse lower-quality experimental data. Irregular leading edges are accounted for by approximating the front by a piecewise constant function, which is constant over windows with a fixed size, w^*. We assume that within each window, the contour moves with constant speed in the perpendicular direction until the left and right leading edges meet. The migration in the scratch assay is characterized by a series of linear approximations to the interface's position over time in these windows.

The paper is organized as follows: in §2.1, we describe our experimental system and in §2.2, we present the agent-based model that we use to simulate the *in vitro* process. In §2.4, we introduce the new migration quantification method for scratch assays and describe the two quantification methods to which we compare it: the *percentage wound area method*, which is widely used, and the *closure rate method*, reviewed in [13]. In §3.1.1, we investigate how the velocity distribution, determined by our quantification method, is affected by cell migration and proliferation. In §3.1.2, we show that the method correctly classifies cells with different migration and proliferation parameters. In §3.1.3, we show the statistical comparison against the other methods. In §3.2.3, we present the results of applying the three methods to an experimental dataset. Finally in §4, we discuss our results and present our conclusions.

2. System and methods

2.1. Cell culture and wound healing assay

Six site-specific mutations in a latent transcription factor that regulate downstream genes involved in essential biological processes, including migration, were generated. Mutants S1, S2, S3, S4, S5 and S6 were then transduced into a human renal carcinoma cell line, 769-P (ATCC CRL-1933), through lentiviral particles. The 769-P mutants were cultured in Dulbecco's modified Eagle's medium (DMEM) (#42430, Gibco) supplemented with 10% of fetal bovine serum (FBS) (#10270, Gibco), 1% of sodium pyruvate solution 100 mM (#03-042-1B, Biological Industries) and 1% of antibiotic–antimycotic solution 100× (#15240, Gibco). Cells were maintained at 37°C in 5% CO_2.

For the wound healing assay, the 769-P mutants (S1–S6) were seeded at 0.025×10^6 cells per well in a two-well silicone insert with a defined cell-free gap (Ibidi #81176, Germany), incubated and allowed to grow for 48 h. Once the cells reached 100% confluence, the culture insert was removed and the area that remained clear of cells was quantified for 24 h using the Live Cell-R Station (Olympus). Digital images were obtained every 30 min.

Data consisted of 24 wound healing assays: four replicates for each of the six groups (S1–S6). Each assay consisted of 48 images. The imaged region size was $500 \times 500\ \mu m^2$.

2.2. Agent-based model of the scratch assay

We consider an agent-based model that has been previously used to simulate *in vitro* cell cultures [21–23]. The simulation domain is a two-dimensional square lattice, with the same dimensions as the experimental images: $[0, D] \times [0, D]$ where $D = 500\ \mu m$. The lattice spacing, Δ, which is interpreted as the average cell diameter, is set to $10\ \mu m$ unless otherwise specified.

In this model, each agent can either proliferate or move within the simulation domain. We consider an end time of $T = 24$ h and an update time of $\tau = 0.1$ h. We include crowding effects by assuming that each lattice site is occupied by at most one cell. A cell with centre at (x, y) is said to be at (x, y). Zero flux boundary conditions are imposed. At each update time, agents move and/or proliferate with migration and proliferation probabilities p_m and p_p, respectively. Since typical estimates of the cell doubling time are approximately 15–30 h [24,25], whereas the time required for a cell to move a distance equal to its diameter is of the order of 10 min [26], we consider migration and proliferation probabilities in the ranges $p_m \in [0, 1]$ and $p_p \in [0, 0.01]$, respectively. The simulation algorithm and typical parameter values are presented in the electronic supplementary material, section S1. In figure 2, we plot the evolution of a typical realization of the agent-based model for which the migration and proliferation parameters are given by $p_m = 0.3$ and $p_p = 0.01$.

2.3. Automatic contour segmentation

The leading edges of the cell monolayers from the experimental images are detected by applying a segmentation algorithm based on the GrowCut method [27]. The method is a robust technique, already employed in several computer vision applications, that performs a binary image segmentation.

The GrowCut algorithm requires the initial specification of a subset of pixels from each type of region: cell monolayer and unoccupied space; these pixels are referred to as *seeds*. The seeds should be located far from the leading edges, where all the pixels of such an area belong to one of the two classes. The algorithm evolves as follows: at each iteration, the pixels surrounding the initial seeds are assigned to one class or the other, adjusting the size of each region. The classification depends on the similarity of the pixel intensity with respect to the pixel intensity of the seeds.

In our implementation, the seeds are chosen as follows: for the cell region, the Canny and Roberts edge contour

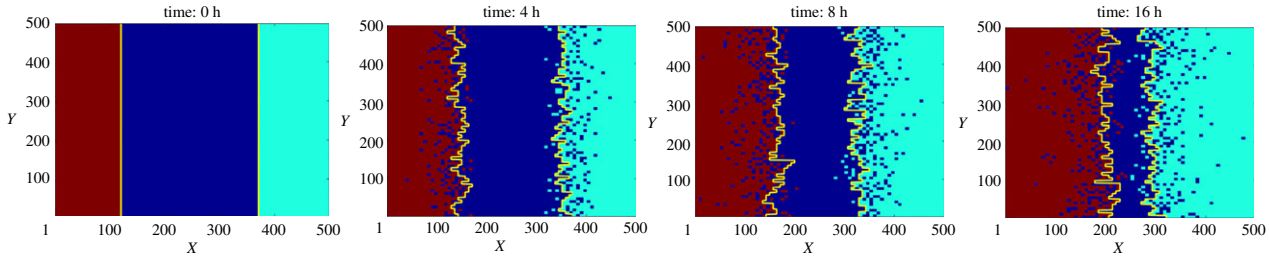

Figure 2. Evolution of an agent-based simulation. We considered an idealized initial condition and fixed the migration and proliferation parameters so that $p_m = 0.3$ and $p_p = 0.01$, respectively. The recolonization of the wounded region is shown at times $t = 0$, 4, 8 and 16 h. For ease of visualization, the two cell monolayers (right and left) are plotted with different colours (red and turquoise), while the area devoid of cells is coloured blue. The leading edges detected by the segmentation algorithm are plotted in yellow. (Online version in colour.)

methods [28,29] are used to select the pixels with the highest variability, corresponding to the cell contours. For the background region, the seeds are set in areas having a low variability, defined as areas in which the pixel intensity has a standard deviation less than 500.

After applying the detection algorithm to each image, we have a record of the positions of the left and the right interfaces at each time where the image was taken. At each vertical position, the interface is considered to be the closest pixel to the wound.

2.4. Migration quantification methods

We first introduce the two established quantification methods for scratch assays. Then, we introduce a new method that quantifies the x-component of the velocity of the leading edge of the cell monolayer.

2.4.1. Area method

One of the most widely used quantification methods, which we term the *area method*, assesses the migration in an indirect manner. During an experiment, the wound area percentage, $\hat{A}(t)$, is tracked:

$$\hat{A}(t) := \frac{A(t)}{A(0)} \times 100\%,$$

where $A(t)$ is the wound area at time t and $A(0)$ is its initial area. The migration rate is then indirectly evaluated as the percentage wound area at a specific time point.

2.4.2. Closure rate method

In [13], cell migration is quantified by assuming that the wound area reduces linearly over time. We refer to this method as the *closure rate method*. The change in wound area $A(t)$ is first approximated by a linear function:

$$A(t) \approx m \times t + b, \tag{2.1}$$

where m and b are real scalars. The wound area is assumed to be the length of the field-of-view (l) times the width of the gap ($W(t)$). Since l is constant during the course of the experiment, equation (2.1) becomes:

$$\frac{\mathrm{d}A}{\mathrm{d}t} \approx l \times \frac{\mathrm{d}W}{\mathrm{d}t}. \tag{2.2}$$

The migration rate, C_r, is defined to be half of the width closure rate

$$C_r := \frac{1}{2}\frac{\mathrm{d}W}{\mathrm{d}t}. \tag{2.3}$$

Combining equations (2.2) and (2.3), we have

$$C_r = \frac{|m|}{2 \times l}. \tag{2.4}$$

2.5. Proposed quantification method: monolayer edge velocimetry

We propose a new strategy for quantifying front migration in a scratch assay using a set of representative velocities. We denote by $t_0, \ldots, t_N$, the times at which data are collected. Let $X \times Y$ represent the square domain of the processed image, $X = Y = \{1, \ldots, D\}$ where D is the number of pixels. For each $j \in Y = \{1, \ldots, D\}$, we denote the interface position in the horizontal direction, at the $j-$th vertical position and at time point t_n, as $i_j(t_n)$ where $1 \leq i_j \leq D$. See figure 3*a* for a schematic representation.

To determine the velocities, we assume a linear approximation to the front position over time for a window size w. The linear approximation is determined in two steps:

(1) First, the front position is approximated for the window size, w. Y is divided into $M = D/w$ segments denoted Y_s, $1 \leq s \leq M$, each of length w. The front position $\hat{i}_s$ in each segment Y_s is approximated by its mean position,

$$\hat{i}_s(t_n) = \langle i_j(t_n) \rangle_{i_j \in Y_s}. \tag{2.5}$$

This procedure is illustrated in figure 3*b*.

(2) The dynamics of the front position in each window is approximated by linear regression, so that

$$\hat{i}_s(t_n) \approx m_s t_n + b_s. \tag{2.6}$$

In figure 3*c*, the dotted lines indicate how the actual front position changes over time at selected y-coordinates; the dashed lines represent the corresponding linear approximations for a window of size $w = 16$.

By performing this approximation for the left and right interfaces, we obtain a set of velocities $\{|m_s|\}_{s=1}^{2M}$ to which we refer as the windowed velocities for window size w.

A necessary step in our method is determining the window size to perform the linear approximation (2.6). We observe that as the window size decreases, the fitness of the linear approximation improves. This observation prompts us to consider the smallest window size; however, for window sizes smaller than the average cell size, the left and right windowed velocity distributions are significantly different. This is a finite-size sampling effect, since the scale

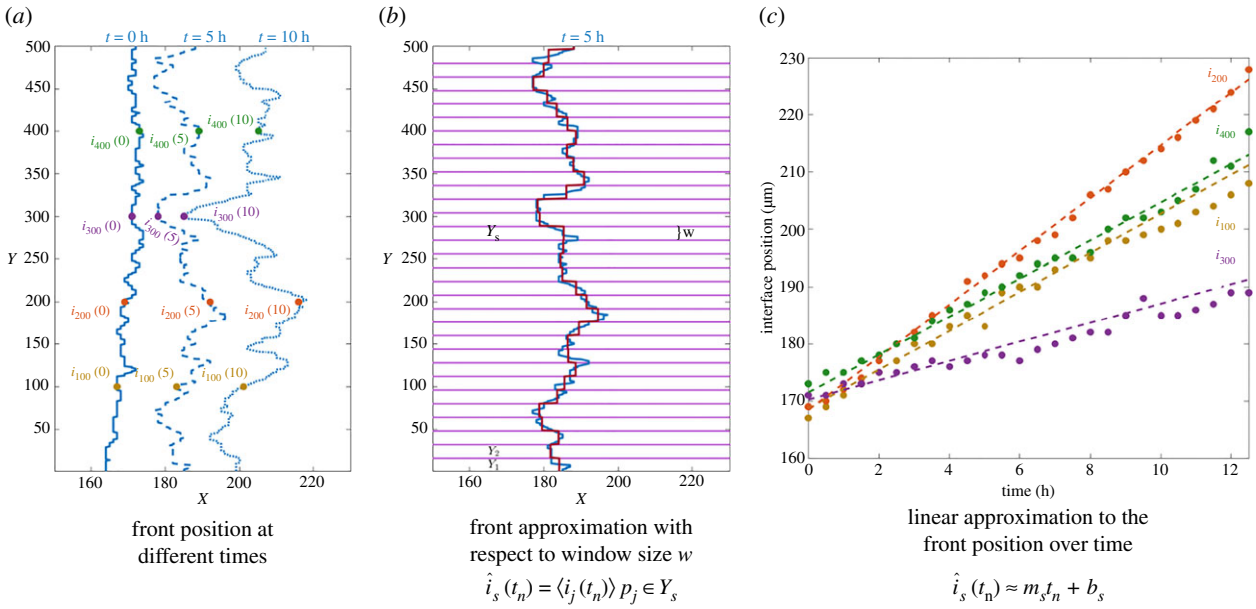

Figure 3. Linear approximation of the front position over time with respect to window size w for one of the scratch assays from the experimental cell groups. (*a*) To introduce the notation, the positions of the left front at times $t = 0$, 5 and 10 h are plotted in blue. The solid line corresponds to $t = 0$ h; the dashed line to 5 h and the dotted line to 10 h. The front positions at the 100, 200, 300 and 400 y-coordinates for these times are plotted: yellow, orange, purple and green, respectively. (*b*) The left front at $t = 5$ h is approximated by a window size w. Y is partitioned into M segments denoted Y_s, $1 \leq s \leq M$, each with length w. A magenta horizontal line delimits each segment. The front position is plotted in blue and the approximated front position, taken as an average over each Y_s, is plotted in red. (*c*) The time evolution of the interfaces at the 100, 200, 300 and 400 y-coordinates and the linear approximation with respect to the window size $w = 16$ are plotted using dotted lines and dashed lines, respectively. The window size $w = 16$ is the window size that maximizes the objective function (2.7). (Online version in colour.)

on which the velocities are quantified is much smaller than the cell size scale. Therefore, the individual velocity of each cell at the front is counted multiple times and its value is over-represented, producing a bias in the overall windowed velocity distribution. To deal with the finite-size sampling effect, we choose a window size for which the left and right windowed velocity distributions are similar. We note that if two different cell types are seeded on either side then the assumption of left and right similarity can no longer be made. However, in the standard experimental set-up of the scratch assay, the left and right interfaces are from the same cell type. A more detailed explanation of why the similarity of the left and right velocity distributions should be considered is included in section S2.1 of the electronic supplementary material.

We use two criteria to select the optimal window size, w^*: (i) fitness of the approximation, and (ii) similarity of the left and right windowed velocity distributions. In more detail, we introduce an objective function, $F(w)$, that has three terms and enables us to find the optimal window size with respect to these two criteria:

$$F(w) = \mathrm{Fit}_{\mathrm{resid}}(w) + \mathrm{Fit}_{\mathrm{Rsquared}}(w) + \mathrm{Fit}_{\mathrm{KS}_{\mathrm{distance}}}(w). \tag{2.7}$$

— $\mathrm{Fit}_{\mathrm{resid}}(w)$ measures the discrepancy between the interface position over time and the linear approximation (equation (2.6)).
— $\mathrm{Fit}_{\mathrm{Rsquared}}(w)$ considers the coefficient of determination, R^2, which describes how well the interface position's variance over time is explained by the linear approximation [30].
— $\mathrm{Fit}_{\mathrm{KS}_{\mathrm{distance}}}(w)$ is a distance function derived from the Kolmogorov–Smirnov (K–S) statistic for the two-sample K–S test [30]; it calculates the distance between the left and right front windowed velocity distributions.

These terms are scaled such that the window size that maximizes the objective function takes into account the trade-off between giving the best fit and having the left and right velocity distributions closest to each other.

The procedure used to determine the optimal window size can be interpreted as a procedure that optimizes the number of velocities needed to characterize the migration. Detailed information about how to modify the objective function when multiple assays are considered can be found in electronic supplementary material, section S2.

The procedure used to determine the set of representative velocities is summarized in algorithm 1.

Algorithm 1. Monolayer edge velocimetry.

1 Determination of the optimal window size for the linear approximation using the objective function (2.7)

$$w^* = \max_{1 \leq w \leq D} F(w) \tag{2.8}$$

where $F(w)$ is given by equation (2.7).

2. Linear approximation, with respect to the window size w^*; indicating how the positions of the left and right interfaces change over time,

$$\hat{i}_s(t_n) \approx m_s t_n + b_s$$

where $\hat{i}_s(t_n) = \langle i_j(t_n) \rangle_{i_j \in Y_s}$, $Y = \bigcup_{s=1}^{M} Y_s$ in which $|Y_s| = w^*$ and $M = D/w^*$.

Output $\{|m_s|\}_{s=1}^{2M}$ is the representative set of velocities that quantify cell migration in the scratch assay.

We refer to the 'monolayer edge velocimetry method' as the MEV method in the rest of the paper.

2.6. Classification test

In order to assess the performance of the three quantification methods in a controlled way, we use the agent-based model to generate *in silico* scratch assays. In particular, we compare the ability of the different methods to distinguish between cell populations with different proliferation and migration parameters. We consider the following classification test:

(1) We fix a focal parameter combination $\hat{P} = (p_{\hat{m}}, p_{\hat{p}}) \in [0, 1] \times [0, 0.01]$ and run n simulations of the agent-based model using these parameter values.
(2) We decompose the parameter space of migration and proliferation probabilities $[0, 1] \times [0, 0.01]$ into a regular 11×11 grid with 121 parameter pairs (p_m, p_p). For each parameter combination, we run n simulations of the agent-based model.
(3) We calculate the cell migration rate in all simulations using the three quantification methods. The migration measurements are windowed velocities, closure rates or areas at specific time points, depending on the quantification method.
(4) For each quantification method, we determine whether the migration measurements of each sampled parameter combination (p_m, p_p) are statistically significantly different from those for the focal parameter pair $\hat{P}$. We perform two tests: the two-sample K–S test and the unpaired two-sample t-test, which we refer to as the K–S test and t-test, respectively. We fix a p-value less than 0.05 to define statistical significance.

We consider a K–S test and a t-test to test for differences at the distribution level and in the mean. We test our data for normality and in case the migration measurements are not normally distributed, we consider a Wilcoxon rank-sum test. We account for stochasticity of the agent-based model by repeating this test 20 times and analyse the mean and variance of the classification results.

When applying the classification test for the MEV method, we consider a global optimal window size for determining the windowed velocities of the simulations. In this way, we obtain the same number of windowed velocities for each simulation. To determine this global optimal window, we consider a weighted sum of the individual objective functions of each simulation (electronic supplementary material, section S2). When applying the classification test to the area method, we must specify the time point at which the wound areas are measured and compared. We fix the comparison time to be half the time it takes the leading edges to touch each other in the first simulation, which is a common choice in an experimental setting.

2.7. Implementation

The segmentation algorithm and the data analysis are implemented in MATLAB version: 9.3.0.713579 (R2017b). The segmentation pipeline uses functions from Matlab's Image Processing Toolbox, the GrowCut algorithm implementation found in http://freesourcecode.net/matlabprojects/56832/growcut-image-segmentation-in-matlab and the normality tests implemented by [31]. The agent-based model is implemented in NetLogo [32]. We do not apply the segmentation algorithm to the *in silico* images so the detection method does not affect the migration rate measurements.

3. Results

3.1. Exploration and validation of quantification method via *in silico* data

We first use the agent-based model to investigate how our quantification method is affected by cell migration and proliferation. Then, by applying the classification test, we investigate how well the method classifies cell populations with different migration and proliferation parameters in comparison with the other quantification methods.

3.1.1. Sensitivity analysis

We investigate how the windowed velocities are affected by the rates of cell migration and proliferation. We vary the migration and proliferation probabilities for fixed initial conditions. We decompose the parameter space of migration and proliferation probabilities $[0, 1] \times [0, 0.01]$ into a regular 11×11 grid with 121 parameter pairs (p_m, p_p). For each parameter combination, 150 simulations were performed and the windowed velocities were calculated. The optimal window was calculated with respect to all simulations for the same parameter combination. In figure 4*a* we present a contour plot of the mean windowed velocity which shows how, as the probabilities increase, the mean velocity increases. A similar trend is observed for the standard deviation (see figure 4*b*).

3.1.2. Classification performance

We suppose that the focal parameter combination, $\hat{P} = (\hat{p}_m, \hat{p}_p)$, takes values in $\{0.1, 0.5, 0.9\} \times \{0.01, 0.05, 0.09\}$ in order to test the classification for small, medium and high values of cell migration and proliferation in our parameter space. We consider $n = 4$ simulations as the sample size for our test, so as to coincide with experimental settings in which four samples are typically used. We repeat the classification test 20 times to produce results that account for the stochasticity of the system.

In figure 5, we plot the results of the mean behaviour of the classification tests when considering the K–S test and the three focal parameter combinations: $\hat{P} = (0.1, 0.01)$, $(0.5, 0.01)$ and $(0.9, 0.01)$. On each plot, the focal parameter combination is indicated by a red circle. At each position (p_m, p_p), we plot a circle whose colour corresponds to the percentage of times the migration measurements of that parameter pair are statistically significantly different to those for the focal parameters $\hat{P}$ with respect to the colourbar at the left of the plots. For parameter pairs different from the focal parameter, $(p_m, p_p) \neq \hat{P}$, the difference between 100% and the percentage of times the migration measurements of that parameter pair are statistically significantly different to those for the focal parameters $\hat{P}$, is an indication of the presence of false negative results. For the focal parameter, $(p_m, p_p) = \hat{P}$, if this percentage is higher than 0% then it indicates the presence of false positive results. We note that for $\hat{P} = (0.1, 0.01)$, the method does not make false negative results: the K–S test indicates that the windowed velocities from simulations of parameter pairs different from the focal parameters, $(p_m, p_p) \neq \hat{P}$, are statistically significantly different to the windowed velocities from simulations of the

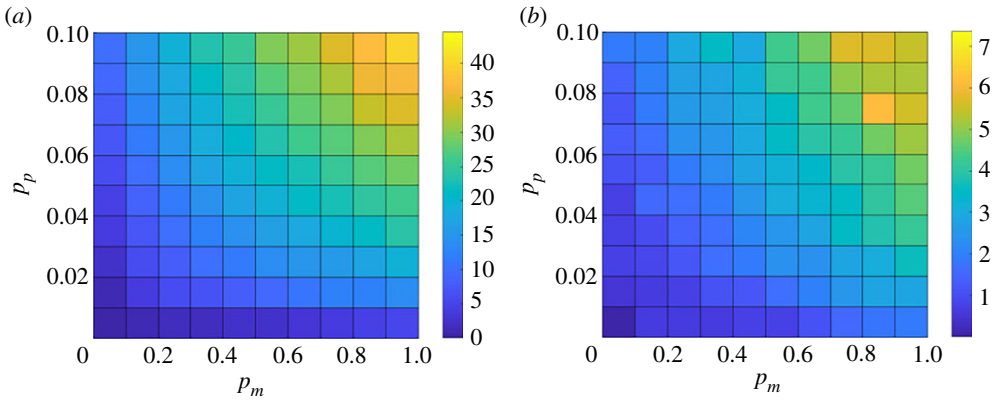

Figure 4. Sensitivity analysis of the agent-based model. We analyse the variability of the windowed velocities with respect to the proliferation and migration probabilities (p_m, p_p) $\in$ [0, 1] $\times$ [0, 0.1]. In (*a*) and (*b*), we plot the mean and the standard deviation of windowed velocities of 150 simulations under each of these 121 parameter pairs. (Online version in colour.)

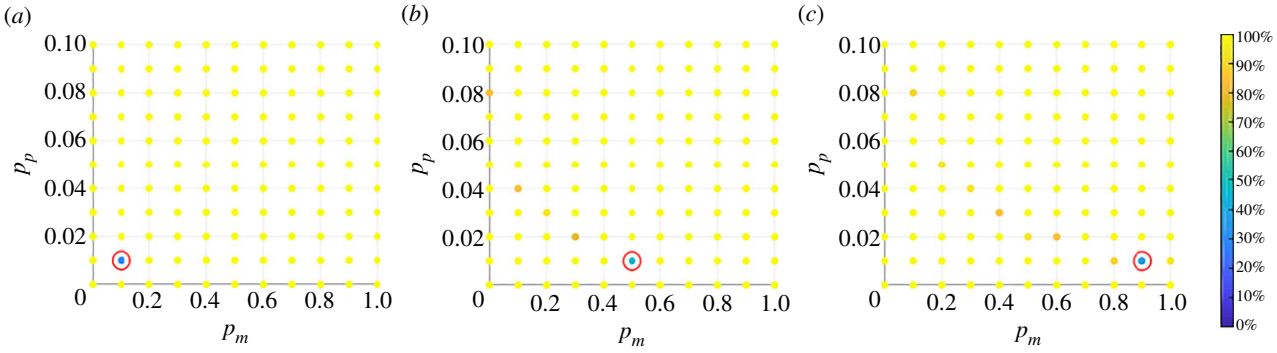

Figure 5. Plots of the mean behaviour of the classification tests for the monolayer edge velocimetry method. The classification tests are performed by considering a K–S test, a sample set of $n = 4$ simulations and the focal parameters (*a*) $\hat{P} = (0.1, 0.01)$, (*b*) $\hat{P} = (0.5, 0.01)$ and (*c*) $\hat{P} = (0.9, 0.01)$. In each plot at each parameter pair (p_m, p_p), the colour of the circle denotes the percentage of times the migration measurements of that parameter pair are statistically significantly different to those for the focal parameter $\hat{P}$. We indicate the focal parameter pair with a red circle. The plots illustrate how the classification performance of the method varies as the migration parameter varies. The method performs better when the migration parameter is small. (Online version in colour.)

focal parameter pair 100% of the time (figure 5*a*). For $\hat{P} = (0.5, 0.01)$, there are four parameter pairs for which the velocities were 80%, 85%, 85% and 95% times statistically significantly different to those for the focal parameter (figure 5*b*). For $\hat{P} = (0.9, 0.01)$, the number of parameter pairs for which the percentage is not 100% increases (figure 5*c*). We observe that as the migration rate increases, the classification performance worsens. The intra-sample difference is accounted for when considering the classification tests for the parameter pair $(p_m, p_p) = \hat{P}$. We observe that the method gives false positive results fewer than 34% of the time. This percentage decreases as the proliferation probability increases (see electronic supplementary material, section S3).

3.1.3. Comparison with standard migration quantification methods

We compare the classification performance of the MEV method with the closure rate and the area methods [3,10]. As before, the focal parameter combination, $\hat{P}$, takes values in $\{0.1, 0.5, 0.9\} \times \{0.01, 0.05, 0.09\}$. We consider $n = 4$ simulations as the sample size and repeat the classification test 20 times.

In figure 6, we plot the mean behaviour of the classification tests for the three quantification methods by applying the K–S test and the focal parameter combinations $\hat{P} = (0.1, 0.01)$, (0.5, 0.01) and (0.9, 0.01). We observe that for a focal parameter pair, the MEV method yields fewer incorrect classifications. We also observe that as the proliferation rate increases, the percentage number of incorrect classifications increases for the three methods.

The results of the classification tests for all other focal parameter combinations in $\{0.1, 0.5, 0.9\} \times \{0.01, 0.05, 0.09\}$ are presented in the electronic supplementary material, section S3. Overall, we observe that our method outperforms the closure rate and the area method. For all focal parameter combinations tested, the MEV method yields a greater percentage of correct classifications. The performance of the area method is the worst while the performance of the closure rate method is intermediate between our method and the area method. The performance of all three methods declines as the values of the migration and proliferation rates of the focal parameters $\hat{P}$ increase. The optimal window sizes for each classification test are of similar size as the cell diameter (results not shown).

3.2. Application of the quantification methods to *in vitro* data

Having tested the quantification methods on *in silico* data, we now use them to analyse experimental data. We first detect the position of the leading edges from the wound healing images

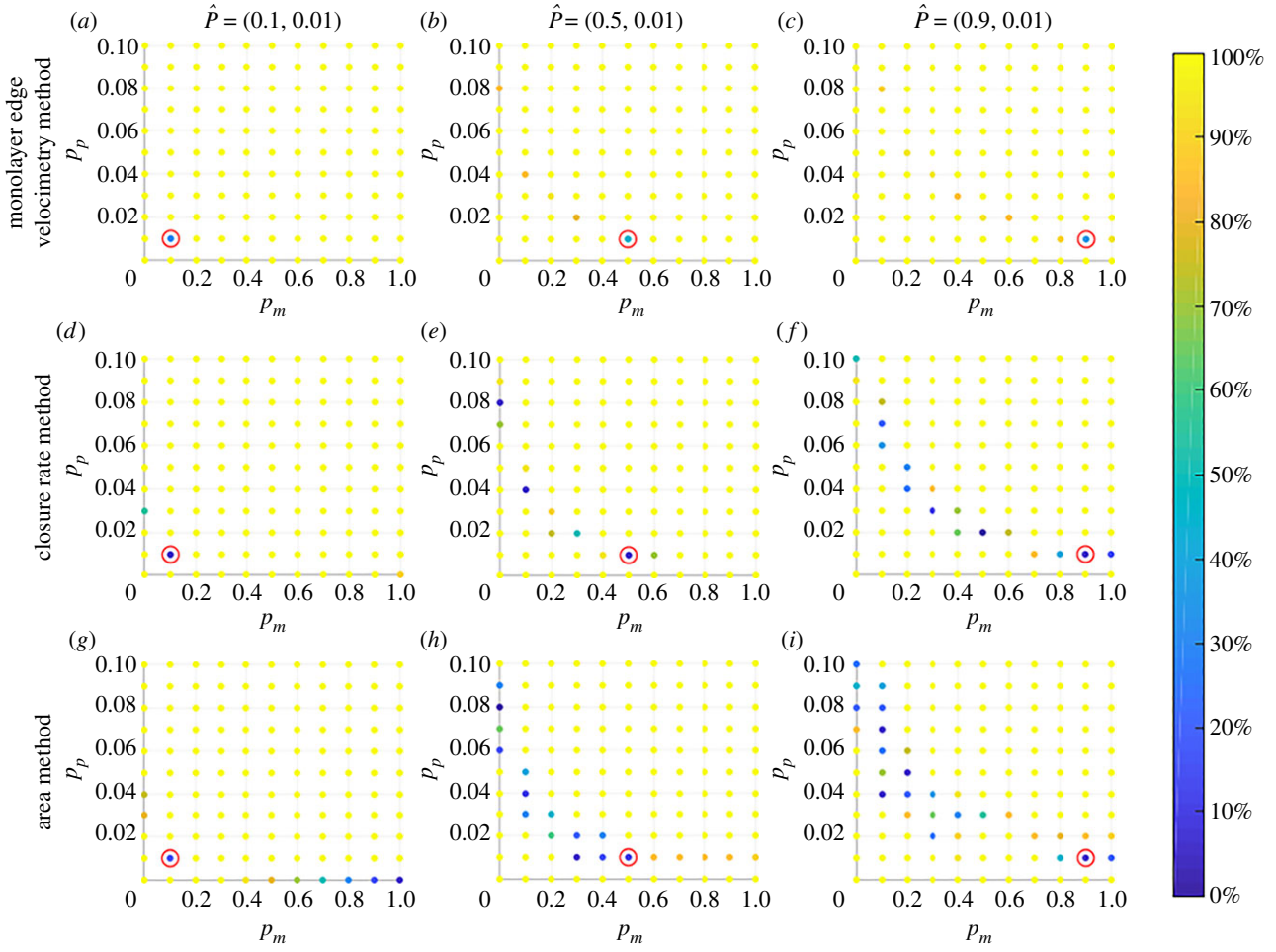

Figure 6. Series of plots showing how the performance of the three quantification methods changes as the migration rate of the focal parameters varies. In each plot, the colour of the circle at each parameter pair (p_m, p_p) indicates the percentage of times the migration measurements associated with the parameter pair are statistically significantly different from those associated with the focal parameters $\hat{P}$. The focal parameters $\hat{P}$ are indicated by a red circle. The results reveal that the monolayer edge velocimetry method yields a better statistical classification than the other methods. We note also the performance of all three methods declines as the migration rate of the focal parameters $\hat{P}$ increases. (Online version in colour.)

taken during the course of the experiments. We then quantify the migration rates using the three quantification methods and analyse the statistical classification.

3.2.1. Image segmentation

After applying the segmentation algorithm, the front of the cell monolayer is detected for each time-lapse image. In figure 1, we present the time-lapse data of a representative scratch from each cell group (S1–S6).

3.2.2. Quantification method results

We quantify the migration velocity of scratch assays for the different cell types using the MEV method. We determine the global optimal window by calculating the objective function for the 24 scratch assays. We vary the window size w from 1 to 500 µm with a step size of 1 µm and use equation (2.7) to calculate the objective function $F(w)$. The objective function and the three fitness functions that contribute to its calculation are shown in the electronic supplementary material, section S4. The maximum value is attained for a window size of 16 µm. For a fixed window size ($w = 16$ µm), we use a linear approximation to describe the position over time of the fronts and determine the 32 representative windowed velocities for each scratch assay and visualize their boxplots in figure 7.

3.2.3. Statistical classification via the local quantification method

After grouping the velocities of scratch assays from the same cell type, the migration rate of each cell group is represented by 256 velocities. The boxplots associated with the velocity distributions for the six groups are shown in figure 8*a*. To determine how different the migration rate of cell group S1 is from the others, we perform a K–S test to test the null hypothesis that the velocities from the two groups come from the same distribution. The null hypothesis was rejected for groups S2, S3 and S4 with statistical significance level of $p_{\text{value}} \leq 0.0001$. The null hypothesis was rejected for group S6 with statistical significance level of $p_{\text{value}} \leq 0.05$. For group S5, the null hypothesis was not rejected. We performed a *t*-test between S1 and each of the other groups to determine whether the mean difference is statistically significant. The mean difference between the velocities for cell groups S1 and S2, S3 and S4 is statistically significant at the 0.0001 level. There was statistical significance in the mean difference with respect to S6 at the 0.05 significance level. The statistical results for the K–S tests and *t*-tests are reported in figure 8*a*.

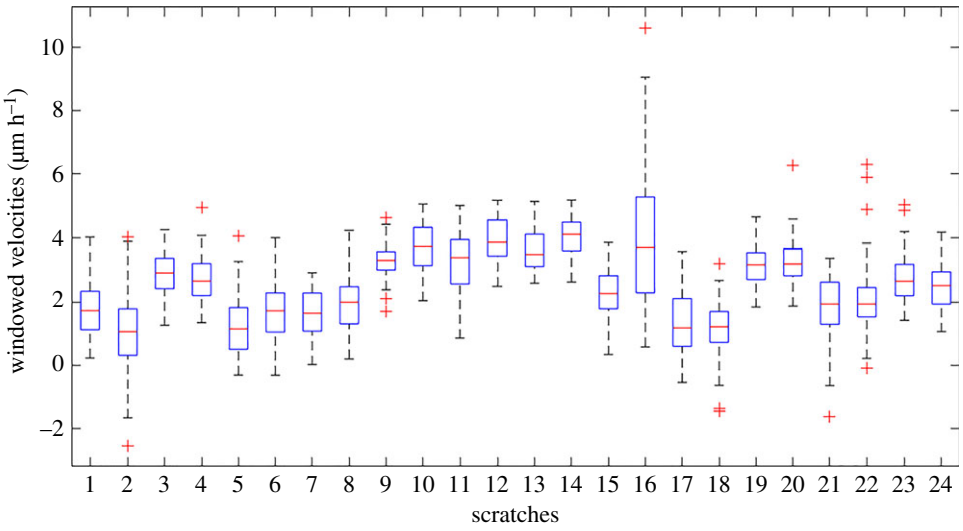

Figure 7. Boxplots of the windowed velocities with respect to the optimal window size of 16 μm for each experimental scratch assay. (Online version in colour.)

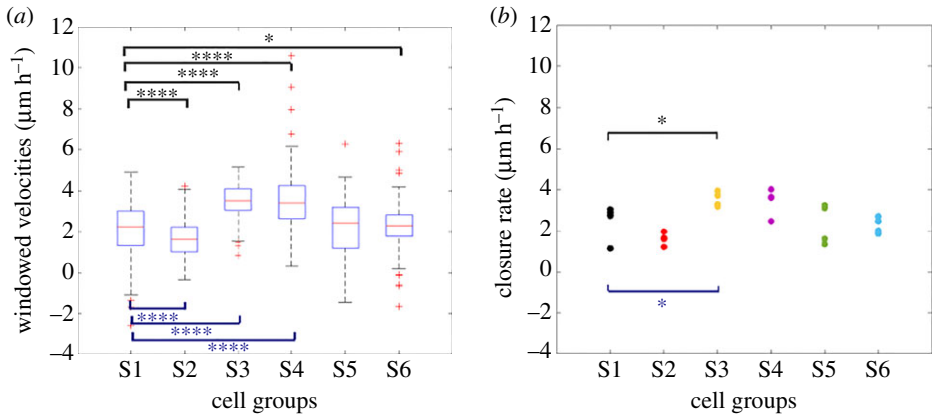

Figure 8. Statistical analysis of the experimental data using the velocity and the closure rate method. First, the migration measurements are grouped into the six different groups (S1–S6). The windowed velocities and the closure rates for the cell groups are plotted in (a), (b). respectively. Above the data, in black, we have reported the statistical significance results from performing a K–S test with respect to the S1 group. Below the data, we have done the same for the *t*-tests. Considering the windowed velocities, with respect to the K–S test and *t*-test, the null hypothesis was rejected testing group S1 against groups S2, S3 and S4 at the 0.001 significance level. Performing the statistical tests with the closure rate measurements, the null hypothesis was rejected at the significance level of 0.05 between S1 and S3. The statistical significance level is decoded in the symbols: $*p_{\text{value}} \leq 0.05$, $**p_{\text{value}} \leq 0.01$, $***p_{\text{value}} \leq 0.001$ and $****p_{\text{value}} \leq 0.0001$. (Online version in colour.)

The exact value of the p_{value} for each test is reported in the electronic supplementary material, section S5.

3.2.4. Statistical comparison to standard migration quantification methods

We now compare the statistical results of our quantification method against those for the area and closure rate methods. In figure 8*b*, we plot the closure rates of each group and report the results from performing the K–S test and *t*-test between S1 and the other groups. S3 was the only group for which the null hypothesis of the K–S test and the *t*-test was rejected at the 0.05 significance level. When we performed the statistical tests for the percentage area measurements, no significant difference was found. In section S5 of the electronic supplementary material, we include the results of the K–S and *t*-tests for the percentage wound area measurements.

4. Discussion and conclusions

In this work, we have introduced a new migration quantification method for scratch assays that characterizes the horizontal component of the front velocity of cell monolayers. The method involves three steps: (1) determination of an optimal window w^* with which to approximate the cell front by a function which is piecewise constant in segments of length w^*; (2) approximation of the interface with respect to the window size w^* at each time point and (3) linear approximation of the position over time of the interface in each of these windows. In this way, we characterize cell migration in the scratch assay by the slopes of a series of linear approximations to the interface position over time in these windows. The optimal window is chosen to be the one that best fits a constant velocity profile and for which the left and right front velocities can be considered to be samples of the same distribution.

By considering an agent-based model that mimics the scratch assay, we tested the ability of our quantification method to distinguish between cell lines with known cell migration and proliferation rates. As the migration and proliferation rates increased, the mean and variance of the windowed velocities increased. This was an expected behaviour since migration and proliferation promote the interface velocity and the variance of the system increases as the migration and proliferation rates increase. By comparing

our quantification method with two existing methods, we observed that our method outperforms both since it yielded a greater percentage of correct classifications than the other methods across a range of parameter values. We noticed that our method made significantly fewer statistical errors than the two other tested methods. Despite being widely used, the performance of the area method was the worst, while the performance of the closure rate method was intermediate between our method and the area method. The poor performance of the area method is due to the presence of irregular cell-free areas and to the indirect quantification of migration by a single time point measurement. The poor performance of the closure rate method is also related to the irregularities in the data since the closure rate method is equivalent to quantifying the migration by the slope of the linear approximation to the mean position of the interface over time.

After showing that our quantification method performed better on *in silico* data, we then used it to analyse our experimental dataset. We calculated an optimal window size of 16 µm, which is of the same order as the mean cell diameter size, and then determined the corresponding windowed horizontal velocities. By performing two-sample K–S and unpaired two-sample *t*-tests, we identified a statistically significant difference between the S1 group and groups S2–S4. The K–S test also indicated statistically significant differences with respect to group S6. We used these two tests as we wanted to detect differences at the distribution level (through the K–S test) and at the mean level (through the *t*-test). The closure rate method only detected statistically significant differences between S1 and S3. The closure rate data are of poor quality: more samples or better quality ones are needed to analyse the migration rate with this method. The area method was unable to detect any statistically significant differences in the dataset. Even when we tried different time points, there was no significant difference. We observed that the S1 cell group also exhibited the highest levels of expression of target genes associated with malignancy and poor prognosis, when analysed by qRT-PCR techniques (data not shown) in agreement with the detected significant differences in migration.

This study has some limitations which could be addressed in future work. For the *in vitro* experiments, the scratch was created by the removal of silicone inserts. It has been observed that the removal of silicone inserts can damage the culture surface coating and affect the cell migration rate [33]. We assume this effect is present in all cell samples so the comparative migration analysis performed by the quantification methods is not affected. Using our quantification method, we would be able to establish how the different procedures for creating the scratch affect migration rates. The statistical performance of our quantification method can be further validated on publicly available wound healing experiment datasets such as those in [34], which provide sets of assays and replicates under different experimental conditions. Currently our quantification method does not take into consideration the intra-group and inter-sample variances of the windowed velocities. In spite of that the classification performance of our quantification method is superior to the area and the closure rate method. The intra-group and inter-sample variances will be taken into consideration in the statistical assessment of the method in a future work. In this study, the agent-based model accounted solely for proliferation and migration events. Additional interactions could be included to give a more realistic description of the scratch assay and the impact of how these factors affect the quantification method could be assessed. The quantification algorithm assumes a linear approximation of the horizontal cell monolayer displacement. Our method could be adjusted to account for an initial phase during which the cells react to the presence of the wound, so the cell monolayer front position over time can be fitted to a Richards function, a non-symmetrical sigmoid function, as in [9]. Currently the method does not address image boundary effects that could potentially affect the quantification. The method could be improved to allow it to deal with the image boundary in a more precise way. One of the drawbacks of our quantification method is the uncertainty in the optimal window size since it depends on the samples. However, in our study, we found that the optimal window size is of the order of the mean cell diameter and the statistical power and measurements of the quantification method are the same for window sizes of the same order (results not shown). If the mean cell diameter is known, then the optimization procedure can be omitted and the linear approximation can be performed using the mean cell diameter as the window size. The framework can also be extended to consider a time-dependent velocity field across the full monolayer, such as cell image velocimetry (CIV) [15]. The challenge in this case would be to determine to which measurements we should apply statistical tests to detect significant differences in migration rates.

In summary, we have introduced a new method for migration quantification of typical scratch assay data, which can be of low quality. Many of the challenges we have overcome with our method could be avoided through improved experimental design. However, the latter would require: repeating the experiment or using more sophisticated experimental tools to create the same degree of confluence and uniform 'wounds'. These are costly solutions. We note that our quantification method can be applied to the existing data. Furthermore, through the classification test based on *in silico* data, we show that even when the quality of the scratches is ideal, our quantification method is better at detecting differences in migration than the other standard methods. While generalization to other nonlinear wound models is not clear, e.g. circular model wounds, the proposed method shows that determining the velocity field along the cell front is sufficient to characterize the migration.

Data accessibility. The source code and the implementation of the algorithm as a GUI along with an example dataset and user instructions, are available at https://bitbucket.org/anavictoria-ponce/local_migration_quantification_scratch_assays/src/master/. The datasets are available at https://ganymed.math.uni-heidelberg.de/victoria/supplementary_data_migration_quantification_scratch_assays.shtml.

Authors' contributions. T.A., A.M. and S.B. designed and coordinated the study. A.V.P.B. developed the agent-based model and performed the processing and analysis of the data. S.B. and A.V.P.B. designed and developed the image processing pipeline. A.M. designed the experiments, while E.S. and J.A. performed them. H.M.B., P.K.M., T.C. and T.A. contributed to the analysis and interpretation of results. A.V.P.B. wrote the paper, on which all other authors commented and made revisions. All authors gave final approval for publication.

Competing interests. We declare we have no competing interests.

Funding. This work was supported by the Heidelberg Graduate School of Mathematical and Computational Methods for the Sciences [DFG grant no. GSC 220 in the German Universities Excellence Initiative to A.V.P.B.]; Mathematics for Industry Network [COST Action TD1409 short-term scientific missions grant to A.V.P.B.]; Consejo Nacional

de Ciencia y Tecnología [411678 to J.A.]; Ministerio de Ciencia e Innovación [TIN2015-66951-C2-1-R and SGR 1742 to S.B., SAF2017-89989-R and SAF2014-59945-R to A.M.]; Red de Investigación Renal REDinREN [12/0021/0013 to A.M.]; the CERCA Programme of the Generalitat de Catalunya to T.A.; Ministerio de Economía y Competitividad [MTM2015-71509-C2-1-R and MDM-2014-0445 to T.A.] and Agència de Gestió de Ajuts Universitaris i Recerca [2014SGR1307 to T.A.].

Acknowledgements. A.V.P.B. would like to thank Isabel Serra Mochales, Matthew Simpson and Andreas Spitz for helpful discussions. We would like to thank Guillem Perez for being the initial promoter of this collaboration.

References

1. Friedl P, Gilmour D. 2009 Collective cell migration in morphogenesis, regeneration and cancer. *Nat. Rev. Mol. Cell Biol.* **10**, 445–457. (doi:10.1038/nrm2720)
2. Li L, He Y, Zhao M, Jiang J. 2013 Collective cell migration: implications for wound healing and cancer invasion. *Burns Trauma* **1**, 21. (doi:10.4103/2321-3868.113331)
3. Grada A, Otero-Vinas M, Prieto-Castrillo F, Obagi Z, Falanga V. 2017 Research techniques made simple: analysis of collective cell migration using the wound healing assay. *J. Investig. Dermatol.* **137**, e11–e16. (doi:10.1016/j.jid.2016.11.020)
4. Kramer N, Walzl A, Unger C, Rosner M, Krupitza G, Hengstschläger M, Dolznig H. 2013 *In vitro* cell migration and invasion assays. *Mut. Res./Rev. Mut. Res.* **752**, 10–24. (doi:10.1016/j.mrrev.2012.08.001)
5. Liang C-C, Park AY, Guan J-L. 2007 *In vitro* scratch assay: a convenient and inexpensive method for analysis of cell migration *in vitro*. *Nat. Protoc.* **2**, 329–333. (doi:10.1038/nprot.2007.30)
6. Simpson KJ, Selfors LM, Bui J, Reynolds A, Leake D, Khvorova A, Brugge JS. 2008 Identification of genes that regulate epithelial cell migration using an siRNA screening approach. *Nat. Cell Biol.* **10**, 1027–1038. (doi:10.1038/ncb1762)
7. Walter MNM, Wright KT, Fuller HR, MacNeil SM, Johnson WEB. 2010 Mesenchymal stem cell-conditioned medium accelerates skin wound healing: an *in vitro* study of fibroblast and keratinocyte scratch assays. *Exp. Cell Res.* **316**, 1271–1281. (doi:10.1016/j.yexcr.2010.02.026)
8. Decaestecker C, Debeir O, Van Ham P., Kiss R. 2007 Can anti-migratory drugs be screened in vitro? A review of 2D and 3D assays for the quantitative analysis of cell migration. *Med. Res. Rev.* **27**, 149–176. (doi:10.1002/(ISSN)1098-1128)
9. Topman G, Sharabani-Yosef O, Gefen A. 2012 A standardized objective method for continuously measuring the kinematics of cultures covering a mechanically damaged site. *Med. Eng. Phys.* **34**, 225–232. (doi:10.1016/j.medengphy.2011.07.014)
10. Masuzzo P, Van Troys M, Ampe C, Martens L. 2016 Taking aim at moving targets in computational cell migration. *Trends Cell Biol.* **26**, 88–110. (doi:10.1016/j.tcb.2015.09.003)
11. Ranzato E, Martinotti S, Burlando B. 2011 Wound healing properties of jojoba liquid wax: an *in vitro* study. *J. Ethnopharmacol.* **134**, 443–449. (doi:10.1016/j.jep.2010.12.042)
12. Büth H, Buttigieg PL, Ostafe R, Rehders M, Dannenmann SR, Schaschke N, Stark H-J, Boukamp P, Brix K. 2007 Cathepsin B is essential for regeneration of scratch-wounded normal human epidermal keratinocytes. *Eur. J. Cell Biol.* **86**, 747–761. (doi:10.1016/j.ejcb.2007.03.009)
13. Jonkman JEN, Cathcart JA, Xu F, Bartolini ME, Amon JE, Stevens KM, Colarusso P. 2014 An introduction to the wound healing assay using live-cell microscopy. *Cell Adh. Migr.* **8**, 440–451. (doi:10.4161/cam.36224)
14. Maška M *et al.* 2014 A benchmark for comparison of cell tracking algorithms. *Bioinformatics* **30**, 1609–1617. (doi:10.1093/bioinformatics/btu080)
15. Milde F, Franco D, Ferrari A, Kurtcuoglu V, Poulikakos D, Koumoutsakos P. 2012 Cell image velocimetry (CIV): boosting the automated quantification of cell migration in wound healing assays. *Integr. Biol.* **4**, 1437–1447. (doi:10.1039/c2ib20113e)
16. Ashby WJ, Zijlstra A. 2012 Established and novel methods of interrogating two-dimensional cell migration. *Integr. Biol.* **4**, 1338–1350. (doi:10.1039/c2ib20154b)
17. Jin W, Shah ET, Penington CJ, McCue SW, Chopin LK, Simpson MJ. 2016 Reproducibility of scratch assays is affected by the initial degree of confluence: experiments, modelling and model selection. *J. Theor. Biol.* **390**, 136–145. (doi:10.1016/j.jtbi.2015.10.040)
18. Jin W, Lo K-Y, Chou S-E, McCue SW, Simpson MJ. 2018 The role of initial geometry in experimental models of wound closing. *Chem. Eng. Sci.* **179**, 221–226. (doi:10.1016/j.ces.2018.01.004)
19. Ruiz-Cañada C, Bernabé-García Á, Liarte S, Insausti CL, Angosto D, Moraleda JM, Castellanos G, Nicolás FJ. 2017 Amniotic membrane stimulates cell migration by modulating transforming growth factor-β signaling. *J. Tissue Eng. Regen. Med.* **12**, 808–820. (doi:10.1002/term.2501)
20. Gorshkova I *et al.* 2008 Protein kinase C-ε regulates sphingosine 1-phosphate-mediated migration of human lung endothelial cells through activation of phospholipase D2, protein kinase C-ζ, and Rac1. *J. Biol. Chem.* **283**, 11794–11806. (doi:10.1074/jbc.M800250200)
21. Johnston ST, Ross JV, Binder BJ, McElwain DLS, Haridas P, Simpson MJ. 2016 Quantifying the effect of experimental design choices for *in vitro* scratch assays. *J. Theor. Biol.* **400**, 19–31. (doi:10.1016/j.jtbi.2016.04.012)
22. Johnston ST, Simpson MJ, McElwain DLS. 2014 How much information can be obtained from tracking the position of the leading edge in a scratch assay? *J. R. Soc. Interface* **11**, 20140325. (doi:10.1098/rsif.2014.0325)
23. Simpson MJ, Landman KA, Hughes BD. 2010 Cell invasion with proliferation mechanisms motivated by time-lapse data. *Phys. A* **389**, 3779–3790. (doi:10.1016/j.physa.2010.05.020)
24. Maini PK, McElwain DLS, Leavesley DI. 2004 Traveling wave model to interpret a wound-healing cell migration assay for human peritoneal mesothelial cells. *Tissue Eng.* **10**, 475–482. (doi:10.1089/107632704323061834)
25. Simpson MJ, Treloar KK, Binder BJ, Haridas P, Manton KJ, Leavesley DI, McElwain DLS, Baker RE. 2013 Quantifying the roles of cell motility and cell proliferation in a circular barrier assay. *J. R. Soc. Interface* **10**, 20130007. (doi:10.1098/rsif.2013.0007)
26. Khain E, Katakowski M, Hopkins S, Szalad A, Zheng X, Jiang F, Chopp M. 2011 Collective behavior of brain tumor cells: the role of hypoxia. *Phys. Rev. E* **83**, 031920. (doi:10.1103/PhysRevE.83.031920)
27. Vezhnevets V, Konouchine V. 2005 GrowCut—interactive multi-label N-D image segmentation by cellular automata. In *Proc. Int. Conf .on Computer Graphics and Vision (GRAPHICON) (2005), 20–24 June, Akademgorodok, Novosibirsk, Russia*, pp. 150–156. See http://www.graphicon.ru/oldgr/en/publications/text/gc2005vk.pdf.
28. Canny J. 1987 A computational approach to edge detection. In *Readings in Computer Vision*, pp. 184–203. Amsterdam, The Netherlands: Elsevier.
29. Shrivakshan GT, Chandrasekar C *et al.* 2012 A comparison of various edge detection techniques used in image processing. *Int. J. Comput. Sci. Issues* **9**, 272–276.
30. Heiberger RM, Holland B. 2015 *Statistical analysis and data display: an intermediate course with examples in R*. Berlin, Germany: Springer.
31. Öner M, Kocakoç İD. 2017 A compilation of some popular goodness of fit tests for normal distribution: their algorithms and Matlab codes (Matlab). *J. Mod. Appl. Stat. Methods* **16**, 30.
32. Tisue S, Wilensky U. 2004 NetLogo: a simple environment for modeling complexity. In *Int. Conf. on Complex Systems, Boston, MA*, vol. 21, pp. 16–21. See http://www.ccl.sesp.northwestern.edu/papers/netlogo-iccs2004.pdf.
33. Liarte S, Bernabé-García Á, Armero-Barranco D, Nicolás FJ. 2018 Microscopy based methods for the assessment of epithelial cell migration during *in vitro* wound healing. *J. Vis. Exp.* **131**, e56799. (doi:10.3791/56799)
34. Zaritsky A, Natan S, Kaplan D, Ben-Jacob E, Tsarfaty I. 2015 Live time-lapse dataset of *in vitro* wound healing experiments. *GigaScience* **4**, 8. (doi:10.1186/s13742-015-0049-6)